INTERNATIONAL JOURNAL FOR NUMERICAL METHODS IN FLUIDS
Int. J. Numer. Meth. Fluids 2009; **61**:946–969
Published online 4 February 2009 in Wiley InterScience (www.interscience.wiley.com). DOI: 10.1002/fld.1988

Momentum/continuity coupling with large non-isotropic momentum source terms

J. D. Franklin[1,2] and Joon Sang Lee[1,*,†]

[1]*Department of Mechanical Engineering, Wayne State University, Detroit, MI 48202, U.S.A.*
[2]*Airflow Sciences Corporation, Livonia, MI, U.S.A.*

SUMMARY

Pressure-based methods such as the SIMPLE algorithm are frequently used to determine a coupled solution between the component momentum equations and the continuity equation. This paper presents a colocated variable pressure correction algorithm for control volumes of polyhedral/polygonal cell topologies. The correction method is presented independent of spatial approximation. The presence of non-isotropic momentum source terms is included in the proposed algorithm to ensure its applicability to multi-physics applications such as gas and particulate flows. Two classic validation test cases are included along with a newly proposed test case specific to multiphase flows. The classic validation test cases demonstrate the application of the proposed algorithm on truly arbitrary polygonal/polyhedral cell meshes. A comparison between the current algorithm and commercially available software is made to demonstrate that the proposed algorithm is competitively efficient. The newly proposed test case demonstrates the benefits of the current algorithm when applied to a multiphase flow situation. The numerical results from this case show that the proposed algorithm is more robust than other methods previously proposed. Copyright © 2009 John Wiley & Sons, Ltd.

Received 19 March 2008; Revised 3 September 2008; Accepted 8 November 2008

KEY WORDS: polyhedral; SIMPLE; colocated; incompressible; CFD; laminar; non-isotrophic source term

1. INTRODUCTION

The use of numerical techniques in engineering design is a well established and standard part of today's industrial design process. In particular, fluid flow analysis based on control volume or finite element techniques is now used successfully on a regular basis. Because of this success, engineers continue to push the limits of these techniques by applying them to more complicated geometries. Frequently the overall success of modeling a complex industrial geometry is not limited by the

*Correspondence to: Joon Sang Lee, Department of Mechanical Engineering, Wayne State University, Detroit, MI 48202, U.S.A.
†E-mail: joonlee@wayne.edu

physics of the flow but by the engineers ability to generate a quality mesh in a timely manner. The control volume community has recently responded to these limitations by introducing numerical algorithms applicable to polygonal/polyhedral mesh topologies. This new cell type provides a broad range of cell topologies acceptable to these algorithms and hence greater flexibility for generating quality meshes.

This paper presents a colocated variable pressure correction algorithm based on the SIMPLE technique, made popular by Patankar [1]. The method presented is applicable to polygonal/polyhedral cell topologies and is developed using generalized spatial discretization. A freshly derived form of the pressure correction equation is presented, which includes non-isotropic momentum source terms frequently encountered in multi-physics applications such as multi-phase flows. Several polygonal/polyhedral test cases are presented detailing the application of the proposed algorithm and its improvements to previously published methods.

2. PUBLISHED FORMS OF THE SIMPLE ALGORITHM

The initial SIMPLE algorithm proposed by Patankar [2] has experienced intense scrutiny over the years. This algorithm has proven to be stable and efficient leading virtually all commercial CFD packages to offer some form of this method. Since its introduction, this algorithm has evolved to meet the demands of more complex geometries.

The form of the SIMPLE algorithm presented in this paper introduces the variable m_c. This variable represents a mass imbalance between two velocity fields, one conserving momentum and another conserving mass on a single control volume mesh topology. This variable does not appear in the original line structured form of the SIMPLE algorithm, since the original algorithm employed a staggered grid arrangement where mass conservation is in-forced on the primary mesh topology and each component of the momentum equation is enforced on a separate staggered mesh. This method does not enforce conservation of mass and momentum on a single control volume, but chooses to scatter the m_c imbalance over several mesh topologies.

Chow and Rhie [3] were the first to introduced the m_c term in the framework of a curvilinear colocated line structured grid. This relationship assumed that each momentum equation followed a particular line in the underlying structured mesh. This assumption simplified the relationship between the momentum equation and the pressure correction equation since all face normals are aligned with each momentum equation, see Section 7 for a detailed development of this relationship. The introduction of this term provided a means of stabilizing the coupled solution of the momentum and continuity equation on a single colocated mesh topology.

The colocated form of the SIMPLE algorithm has been extended to unstructured mesh topologies, see [4, 5]. The development of the pressure correction equation by these authors utilized simplified forms of the linearized momentum coefficients since the momentum equation is not aligned with the mesh topology. Mathur and Murthy [4] suggest averaging the linear system momentum coefficients, $A_p^{u_i}$, since these values are isotropic throughout the domain (except in boundary cells). Ferziger and Peric [5] on the other hand suggest using the normal of the coefficient, $A_p^{u_i} \cdot n_i$. Either of these methods have been shown to effectively damp out pressure checker boarding, providing an efficient and reliable method for coupling the momentum and continuity equations.

Date [6] has presented a fluid dynamical view of the m_c term. His analysis accounts for non-isotropic behavior through multidimensional averaging. This method attempts to reconstruct a line structure similar to the structured mesh algorithm through complex interpolations. This

DOI: 10.1002/fld

multidimensional averaging technique results in a dereferenced pressure correction field based on a smoothed pressure field. This smoothed pressure field provides a method of distributing the m_c imbalance during the solution of the pressure correction equation providing the commonly referenced fourth-order damping typically associated with the colocated form of the SIMPLE algorithm, see [5].

From the perspective of multiphase flow one cannot assume that the $A_p^{u_i}$ momentum coefficients will be isotropic and in fact most time will not be. One might argue that it does not matter how this term is approximated since it is only used as a correction and at convergence this approximation will not play a role in the final solution. Snider [7], however, has noted that colocated variable arrangements exhibit instabilities compared with the staggered formulation when applied to multiphase flows. Section 9.2 demonstrates that the method proposed in this paper enhances the stability and convergence of the SIMPLE-based momentum/continuity coupling by treating the $A_p^{u_i}$ terms in a more rigorous form. The proposed form in this paper is compared with the form of [4] when applied to a multiphase application.

3. GOVERNING EQUATIONS

The conservative/integral form of the steady state momentum equations for the Cartesian coordinate system is presented by Ferziger and Peric [5].

$$\int_S \rho u_i (\mathbf{u}\cdot\mathbf{n})\,\mathrm{d}S = \int_S (\mathbf{T}_i\cdot\mathbf{n})\,\mathrm{d}S + \int_{\forall} \mathbf{F}\,\mathrm{d}\forall \tag{1}$$

where the tensor, $(\mathbf{T}_i)$, for a Newtonian fluid has the following form:

$$\mathbf{T}_i = \mu\nabla u_i + \mu(\nabla\mathbf{u})^{\mathrm{T}}\cdot\mathbf{i}_i - (p + \tfrac{2}{3}\mu\nabla\cdot\mathbf{u})\mathbf{i}_i \tag{2}$$

This form of the momentum equation is based on a control volume $\forall$ bounded by a surface S, which has an outward pointing unit normal $\mathbf{n}$. An external momentum force term, $\mathbf{F}$, is included in this form of the momentum equation. The subscript (i) indicates each of the Cartesian components of the momentum equation and the fluid velocity is given the symbol $\mathbf{u}$.

The integral form of the continuity equation is as follows:

$$\int_S \rho(\mathbf{u}\cdot\mathbf{n})\,\mathrm{d}S = 0 \tag{3}$$

4. DISCRETIZATION

4.1. Scalar transport equation

The transport of a scalar, Φ, by means of convection, diffusion, and a volumetric source term is given as follows:

$$\int_S \Phi\rho(\mathbf{u}\cdot\mathbf{n})\,\mathrm{d}S = \int_S \left(\Gamma\frac{\partial\Phi}{\partial n}\right)\mathrm{d}S + \int_{\forall} S_\Phi\,\mathrm{d}\forall \tag{4}$$

DOI: 10.1002/fld

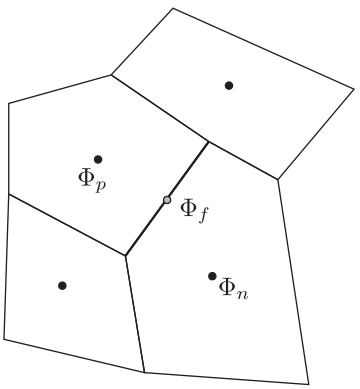

Figure 1. Two-dimensional polygonal cell discretization.

The discretization of this equation follows standard practice. The surface integrals are considered to be a series of semi-planar faces, f, bounding a control volume, $\forbar{V}$.

$$\sum_f \Phi_f \rho(\mathbf{u}_f \cdot \mathbf{n}) A = \sum_f \Gamma_f \left(\frac{\partial \Phi}{\partial n}\right)_f A + S_\Phi \forbar{V} \tag{5}$$

To complete this discretization, spatial approximations are required. These approximations are written implicitly and explicitly in terms of volume-averaged quantities stored at the centroid of each control volume, see Figure 1. For the current development, a linear variation (second-order accurate) is assumed between control volume centroids. The volumetric source term, S_Φ, is written in a linearized form.

4.1.1. Convection term. The left-hand term in Equation (5) is typically referred to as the convection term. This term represents the mass flux of Φ_f passing through face f. There have been many methods proposed in the literature for approximating Φ_f, see [8] for some of the early work in this area and more recently [9, 10]. All of these methods have the same fundamental linearized form about a control volume face and can be generally written as follows:

$$\Phi_f = \underbrace{C^n_{f,\text{implicit}} \Phi_n - C^p_{f,\text{implicit}} \Phi_p}_{\text{implicit}} + \underbrace{C_{f,\text{explicit}}(\Phi)}_{\text{explicit}} \tag{6}$$

where $C^n_{f,\text{implicit}}$ and $C^p_{f,\text{implicit}}$ are the implicit interpolation factors and $C_{f,\text{explicit}}(\Phi)$ is an explicit adjustment to the implicit interpolation, typically a function of the control volume values in the vicinity of face f.

4.1.2. Diffusion term. The first term on the left-hand side of Equation (5) is the diffusion term. It represents the propagation of Φ between control volumes due to spatial gradients. The normal

DOI: 10.1002/fld

gradient across face f can be written in generalized form as follows:

$$\left(\frac{\partial \Phi}{\partial n}\right)_f = \underbrace{D_{f,\text{implicit}}(\Phi_n - \Phi_p)}_{\text{implicit}} + \underbrace{D_{f,\text{explicit}}(\Phi)}_{\text{explicit}} \tag{7}$$

where the implicit portion is written based on the centroidal values on either side of the face and an implicit coefficient, $D_{f,\text{implicit}}$. The explicit function, $D_{f,\text{explicit}}(\Phi)$, is based on a select number of control volume values in the vicinity of face, f. Just as with the convection term many methods have been used to represent this gradient, see [4, 11].

4.1.3. Face centroidal interpolation. The discretization of the scalar value Φ is based on a colocated variable storage scheme. The current development also stores the transport variables such as fluid density and diffusivity at the centroids of the control volumes. Interpolation is used to determine the face values such as the Γ_f coefficient in Equation (5). Simple linear interpolation was originally used with traditional Cartesian structured grids. More complicated mesh topologies have lead to more sophisticated interpolation techniques using shape functions or polynomial approximations such as least squares. Just as with the other terms the face interpolated values will be written in a generalized form:

$$\Gamma_f = \overline{\Gamma} \tag{8}$$

where the over-line represents a general interpolation technique based on the near face control volume values.

4.1.4. Linearized source. To enhance stability proper source term linearization is advisable. Patankar [1] has established some basic rules for the development of well-conditioned linear systems. Rule three recommends the following form for linearized source terms.

$$S_\Phi(\Phi) = S_{\text{explicit}} + S_{\text{implicit}}\Phi_p \tag{9}$$

where the subscript, p, denotes the primary cell variable, Φ_p, located at the control volume centroid. The implicit and explicit portions of the source term are indicated by subscripts, where the implicit portion must always be negative to increase the diagonal dominance of the linear system.

5. MOMENTUM EQUATION

The discretization of the linear momentum equation, Equation (1), in the Cartesian coordinate system has the following form:

$$\sum_f [u_i \rho \mathbf{u}\cdot\mathbf{n}A]_f - \sum_f [A\mu]_f \left(\frac{\partial u_i}{\partial n}\right)_f = \sum_f \left\{ \left[A\mu \frac{\partial u_j}{\partial x_i}\right]_f \cdot \mathbf{n} - \left[A\frac{2}{3}\mu \frac{\partial u_j}{\partial x_j} n_i\right]_f - [Apn_i]_f \right\}_f + F_i \forall \tag{10}$$

DOI: 10.1002/fld

where A is the face surface area, $\mathbf{u}$ is the fluid velocity vector (components u_i), $\mathbf{n}$ is the surface outward pointing unit normal (components n_i), x_i represents each of the Cartesian coordinates and the volumetric force term $\mathbf{F}$ is shown in terms of its Cartesian components F_i. Each component of the momentum equation can be expressed in terms of the standard convection diffusion equation, Equation (5), with the following substitutions:

$$\begin{aligned}
\Phi_f &= u_i \\
\Gamma_f &= \mu \\
\frac{\partial \Phi}{\partial n} &= \frac{\partial u_i}{\partial n} \\
S_\Phi &= \sum_f \left\{ \left[A\mu \frac{\partial u_j}{\partial x_i} \right]_f \cdot \mathbf{n} - \left[A\frac{2}{3}\mu \frac{\partial u_j}{\partial x_j} n_i \right]_f - [Apn_i]_f \right\}_f + F_i \forall
\end{aligned} \tag{11}$$

To ease further manipulation the momentum equation is typically further simplified to the following form:

$$u_{i,p} A_p^{u_i} + \sum_f u_{i,f} A_f^{u_i} = Q^{u_i} - \sum_f [Apn_i]_f \tag{12}$$

where the $A_p^{u_i}$ and $A_f^{u_i}$ terms are collections of the implicit coefficients and the Q^{u_i} represents the explicit terms for each of the u_i momentum equations. The Cartesian velocity components at the centroid of the primary cell are given the symbol $u_{i,p}$ and the notation $u_{i,f}$ denotes the centroidal value connected to the primary cell through face f. The presence of non-isotropic source terms, S_Φ, can lead to a significant variation in $A_p^{u_i}$ and $A_f^{u_i}$. Note also that the explicit pressure force terms are not grouped with the other explicit terms since they require special consideration when coupling with the continuity equation.

The solution of Equation (12) employs relaxation. For this development each momentum equation will have the same relaxation, assigned the symbol α, and will be introduced as follows:

$$\frac{A_p^{u_i}}{\alpha} u_{i,p} + \sum_f u_{i,f} A_f^{u_i} = Q^{u_i} - \sum_f [Apn_i]_f + (1-\alpha)\frac{A_p^{u_i}}{\alpha} u_{i,p}^\circ \tag{13}$$

where $u_{i,p}^\circ$ is some initial velocity.

6. CONTINUITY EQUATION

The discretization of the continuity equation, Equation (3), results in the following relationship:

$$\sum_f \rho_f (\mathbf{u}_f \cdot \mathbf{n}) A = 0 \tag{14}$$

which is simply the sum of the mass flows through each face bounding the primary control volume p.

DOI: 10.1002/fld

7. COUPLING

One technique that has been used extensively to determine a coupled solution between the momentum and continuity equations is the so-called pressure correction technique. Many variations of this technique have been proposed. Patankar [1] and his commonly cited text book is a common reference for the SIMPLE version of this technique. Recently, Date [6] has reviewed this technique from the perspective of colocated variable arrangements.

This pressure projection technique alternates between individual solutions of the momentum equations and a velocity projection relationship, which directs the velocity field toward conservation of mass. This iterative process begins with an estimated pressure field and solves the momentum equations for the Cartesian component velocity field. This velocity is not typically mass conservative, since conservation of momentum does not enforce conservation of mass. The continuity equation is then used to project a new velocity and pressure field, which conserves mass. Typically only a portion of the full correction is taken since several of the correction terms are difficult to calculate and are usually ignored. If this procedure is repeated, however, the amount of the projection tends to zero resulting in a velocity and pressure field satisfying both conservation of mass and momentum.

7.1. Pressure/velocity corrections

The standard notation used when developing a relationship for this technique is as follows:

$$\mathbf{u}_p^{k+1} = \hat{\mathbf{u}}_p^k + \mathbf{u}'_p, \quad p^{k+1} = p^k + p' \tag{15}$$

where each variable represents the following quantities at the centroid of a primary control volume:

- $\mathbf{u}_p^{k+1}$ mass conserving velocity field
- $\hat{\mathbf{u}}_p^k$ momentum conserving velocity field
- $\mathbf{u}'_p$ velocity field adjustment to achieve mass conservation
- p^{k+1} mass conserving pressure field
- p^k assumed pressure field for determining the momentum conserving velocity field $\hat{\mathbf{u}}_f^k$
- p' adjustment to pressure field to achieve mass conserving pressure field.

Conservation of mass, Equation (14), is the starting point for the development of the projection technique. Rewriting this equation using the above notation:

$$\sum_f \rho_f (\mathbf{u}_f^{k+1} \cdot \mathbf{n}) A = \sum_f \rho_f (\overline{\mathbf{u}_p^{k+1}} \cdot \mathbf{n}) A = \sum_f \rho_f (\overline{u_{i,p}^{k+1}} n^i) A = 0 \tag{16}$$

where the face centroidal velocity, u_f^{k+1}, can be expressed in terms of the interpolated cell centroidal velocity, $\overline{\mathbf{u}_p^{k+1}}$.

When the momentum and continuity equations are in balance with the pressure field, the discretized form of the momentum equation can be used to form a relationship for, $u_{i,p}^{k+1}$.

$$u_{i,p}^{k+1} = \frac{1}{A_p^{u_i}} \left(Q^{u_i^k} - \sum_f u_{i,f}^{k+1} A_f^{u_i} - \sum_f [A p^{k+1} n_i]_f \right) \tag{17}$$

DOI: 10.1002/fld

Equation (17) is inserted into Equations (16) and (15), which are used to write the continuity equation in terms of momentum conservative velocities and their corrections.

$$\underbrace{\sum_f \left[A\rho_f \overline{\frac{1}{A_p^{u_i}} \sum_f [Ap' n_i]_f} \right]_f n^i}_{\text{Pressure Correction}} = \underbrace{\sum_f \left[A\rho_f \overline{\left(\frac{1}{A_p^{u_i}} \left(Q^{u_i^k} - \sum_f \hat{u}_{i,f}^k A_f^{u_i} - \sum_f [Ap^k n_i]_f \right) \right)} \right]_f n^i}_{\text{Un-relaxed Momentum Conserving Velocity, } \hat{u}_{i,p}^k}$$
$$\underbrace{- \sum_f \left[A\rho_f \overline{\frac{1}{A_p^{u_i}} \left(\sum_f u'_{i,f} A_f^{u_i} \right)} \right]_f n^i}_{\text{Velocity Correction Term}} \tag{18}$$

The SIMPLE projection variation will be used in the current development, hence, the velocity correction term of Equation (18) will be neglected. Since relaxation is employed when solving the momentum equation, we will replace the unrelaxed velocity relationship in Equation (18) with the relaxed form, Equation (19):

$$\hat{u}_{i,p}^k = \frac{\alpha}{A_p^{u_i}} \left(Q^{u_i^k} - \sum_f \hat{u}_{i,f}^k A_f^{u_i} - \sum_f [Ap^k n_i]_f \right) + (1-\alpha) u_{i,p}^\circ \tag{19}$$

This leads to the standard pressure correction, p', based continuity equation used in SIMPLE-based algorithms. The current form of this equation cannot be discretized to determine the pressure correction, p', distribution for mass conservation, since the pressure correction relationship, the left-hand side of Equation (18), is expressed in terms of interpolated pressure correction values. The following sections outline a method for transforming this relationship into a form which can be used to solve for the p'.

7.2. Pressure gradient manipulation

The surface integrations containing the pressure terms, p' and p^k, can be expressed in terms of gradients by means of Gauss' Theorem:

$$\left(\frac{\partial \phi}{\partial x_i} \right)_p \approx \frac{\int_{\forall} \frac{\partial \phi}{\partial x_i} \mathrm{d}\forall}{\forall} \approx \frac{\sum_f [A\phi n_i]_f}{\forall} \tag{20}$$

which results in the following relationship for a general pressure field p (either p' or p^k):

$$- \sum_f \left[A\rho_f \overline{\frac{1}{A_p^{u_i}} \sum_f [pAn_i]_f} \right]_f n^i = - \sum_f \left[A\rho_f \overline{\frac{\forall}{A_p^{u_i}} \left(\frac{\partial p}{\partial x_i} \right)_p} \right]_f n^i \tag{21}$$

The volume gradient of p interpolated to the cell face does not lend itself to discretization. However, if it were written in terms of a face normal gradient it could be discretize using the

DOI: 10.1002/fld

standard relationship for a normal scalar gradient on a face, see Equation (7). Consider transforming the pressure gradient to a face-based coordinate system. Where the face-based coordinate system is a rotation of the Cartesian coordinate system with axis **n**, **s** and **t**. The **n** axis is aligned normal to the control volume face and the **t** and **s** axis are the tangential coordinate directions on the control volume face.

$$\frac{\partial p}{\partial x_i} = \frac{\partial p}{\partial n} n_i + \frac{\partial p}{\partial t} t_i + \frac{\partial p}{\partial s} s_i \tag{22}$$

Substitution of this relationship and separation into normal and tangential components results in the following relationship, where the tangential components can be shown to be zero and can be eliminated:

$$-\sum_f \left[A \rho_f \overline{\frac{\forall}{A_p^{u_i}} \left(\frac{\partial p}{\partial x_i} \right)_p} \right]_f n^i = \underbrace{-\sum_f \left[A \rho_f \overline{\frac{\forall n_i}{A_p^{u_i}} \left(\frac{\partial p}{\partial n} \right)_p} \right]_f n^i}_{\text{normal}}$$

$$\underbrace{-\sum_f \left[A \rho_f \overline{\frac{\forall}{A_p^{u_i}} \left(\frac{\partial p}{\partial t} t_i + \frac{\partial p}{\partial s} s_i \right)_p} \right]_f n^i}_{\text{tangential}} \tag{23}$$

The interpolated normal gradient can be represented by a direct gradient across each control volume face resulting in a form, which can be discretized using the standard face gradient, Equation (7).

$$-\sum_f \left[A \rho_f \overline{\frac{\forall}{A_p^{u_i}} \left(\frac{\partial p}{\partial x_i} \right)_p} \right]_f n^i = -\sum_f A \rho_f \overline{\frac{\forall n_i n^i}{A_p^{u_i}}} \left(\frac{\partial p}{\partial n} \right)_f \tag{24}$$

7.3. Pressure correction relationship

Equation (18) can be simplified using the assumptions presented in Sections 7.1 and 7.2 to Equation (25), where the assumptions for the pressure have been consistently applied to both the pressure, p^k, and the pressure correction, p':

$$\sum_f \left[A \rho_f \overline{\frac{\forall n_i n^i}{A_p^{u_i}}} \left(\frac{\partial p'}{\partial n} \right)_f \right]_f = \sum_f \left[A \rho_f \overline{\left(\frac{\alpha}{A_p^{u_i}} \left(Q^{u_i^k} - \sum_f \hat{u}_{i,f}^k A_f^{u_i} \right) + (1-\alpha) u_{i,p}^{\circ} \right) n^i} \right]_f$$

$$-\sum_f \left[A \rho_f \alpha \overline{\frac{\forall n_i n^i}{A_p^{u_i}}} \left(\frac{\partial p^k}{\partial n} \right)_f \right]_f \tag{25}$$

DOI: 10.1002/fld

From a data manipulation standpoint it is convenient to note that if the pressure surface integration is added and subtracted from the right-hand side of Equation (25) the relaxed form of the momentum conservative velocity, Equation (19), appears.

$$-\sum_f\left[A\rho_f\frac{\overline{\forall n_i n^i}}{A_p^{u_i}}\left(\frac{\partial p'}{\partial n}\right)_f\right]_f=-\sum_f\left[A\rho_f\underbrace{\overline{\left(\frac{\alpha}{A_p^{u_i}}\left(Q^{u_i^k}-\sum_f\hat{u}_{i,f}^k A_f^{u_i}-\sum_f[Ap^k n_i]_f\right)+(1-\alpha)u_{i,p}^{\circ}\right)}n^i}_{\hat{u}_{i,p}^k}\right]_f$$
$$+\sum_f\left[A\rho_f\underbrace{\alpha\left(\overline{\frac{\forall n_i n^i}{A_p^{u_i}}\left(\frac{\partial p^k}{\partial n}\right)_f}-\overline{\frac{1}{A_p^{u_i}}\sum_f[Ap^k n_i]_f n^i}\right)}_{m_c}\right]_f \tag{26}$$

This substitution results in the commonly referenced stabilization term, m_c. The first form of m_c was introduced by Chow and Rhie [3]. This term is the difference between two methods of representing the normal pressure gradient at the surface of the control volume. One method is simply an interpolated volume-centered pressure gradient and the other is a direct normal gradient. When the pressure field is linear this term will be zero, however, when the pressure field is non-linear then this term will be non-zero and must be accounted for to avoid pressure checker boarding.

7.4. Velocity correction

The m_c stabilization term is included by introducing a mass conservative control surface normal velocity, $u_{f,n}^k$, as suggested by Chow and Rhie [3]. The right-hand side of Equation (26) is used to form

$$u_{f,n}^k=\overline{\hat{u}_{i,p}^k}\cdot n_i+m_c \tag{27}$$

Note that Equation (27) is based on the control volume primary variables, $u_{i,p}^k$ and p^k, and the discretization of the momentum equation. This technique mimics the staggered formulation via interpolation and highlights the inclusion of the m_c term inherent in all SIMPLE-type pressure projection formulations.

Once the primary pressure correction, p'_p, has been computed, via Equation (26), the momentum conserving velocity and pressure fields are corrected as follows:

$$u_{i,p}^{k+1}=\hat{u}_{i,p}^k-\frac{\forall}{A_p^{u_i}}\sum_f[A\overline{p'}n_i]_f \tag{28}$$

$$u_{f,n}^{k+1}=\hat{u}_{f,n}^k-\overline{\frac{\forall n_i n^i}{A_p^{u_i}}\left(\frac{\partial p'}{\partial n}\right)_f} \tag{29}$$

$$p_p^{k+1}=p_p^k+\alpha_{\text{pres}}p'_p \tag{30}$$

Note that cell-centered, $\hat{u}_{i,p}^k$, and face-centered, $u_{f,n}^k$, velocities are corrected separately using pressure gradient treatments consistent with the continuity equation treatment. The pressure is also

DOI: 10.1002/fld

corrected using only a portion of the full correction, α_{pres}, to ensure stability since some of the terms were neglected in the development of the pressure correction relationship.

7.5. Coupling algorithm

The resulting algorithm for the solution of the coupled momentum/continuity relationship can be paraphrased as follows:

1. Guess a value for $u^{\circ}_{i,p}$, $u^{\circ}_{f,n}$ and p.
2. Solve Equation (13) for the momentum conserving velocity, $\hat{u}^{k}_{p}$, using the assumed values from step 1.
3. Solve Equation (26) for the volume-centered pressure correction, p'_{p}.
4. Correct the velocity and pressure via Equations (28), (29) and (30).
5. Return to step 1 using $u^{k+1}_{i,p}$, $u^{k+1}_{f,n}$ and p^{k+1}_{p} as the initial guess values.

8. BOUNDARY CONDITIONS

The application of boundary conditions for the proposed algorithm follow the standard methods used in SIMPLE-based colocated algorithms, see [5]. At wall boundaries, a no-slip condition is imposed in the momentum equation and a Neumann condition, $\partial p'/\partial n = 0$, is applied in the pressure correction equation. Fixed values are used for inflow boundaries in the momentum equations and $\partial p'/\partial n = 0$ in the pressure correction equation. The common practice of zero diffusive flux for constant pressure out flow boundary conditions is used in the momentum equations and a fixed pressure correction of zero, a Dirichlet condition, is used in the pressure correction equation. Symmetry boundary conditions enforce a zero tangential shear and a zero normal flow condition in the momentum equations. Since a symmetry plane implies zero normal flow the pressure correction equation uses the same condition imposed for the wall boundary condition, $\partial p'/\partial n = 0$.

9. RESULTS

The proposed pressure correction algorithm is applied to two classic validation cases and introduces an idealistic multiphase flow case. The classic cases demonstrate that the algorithm is competitive with existing methods and is applied using arbitrary polygonal/polyhedral mesh topologies. The multiphase flow case demonstrates the importance of properly handling the momentum coefficients in the projection algorithm by comparing the proposed algorithm with previously published methods.

The MUSCL algorithm presented by Darwish and Moukalled [10] is used for the generalized convective face value Φ_f, Equation (6). The spatial discretization proposed by Jasak [12] is used for Equations (7) and (8). The same relaxations are used for all cases $\alpha = 0.7$ and $\alpha_{\text{pres}} = 0.3$, following the common rule of maintaining the sum of the two relaxations to 1, see [5]. Zero was assumed as the initial values for all primary variables (velocity and pressure).

DOI: 10.1002/fld

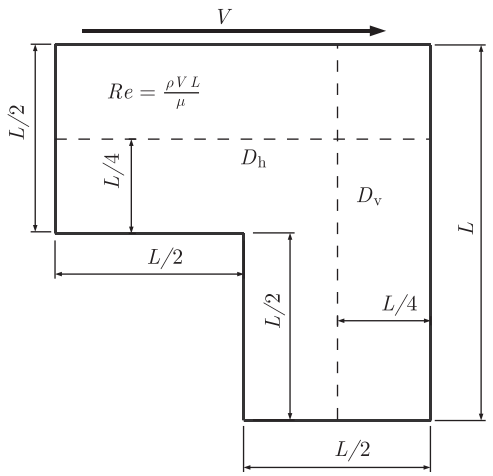

Figure 2. Cavity geometry [13].

The absolute residual, R_Φ, for the momentum equation has been evaluated using Equation (31) and the pressure correction/continuity equation using Equation (32). The iteration process was continued for each model until all residuals dropped below 1.0e−4.

$$R_\Phi = \sum_{\text{cells p}} \left| \sum_f A_f \phi_f + b - A_p \phi_p \right| \tag{31}$$

$$R_{\text{mass}} = \sum_{\text{cells p}} \left| \sum_f u^k_{f,n} \right| \tag{32}$$

9.1. L-shaped cavity

Two-dimensional lid-driven cavities have been used extensively as benchmark problems for momentum/continuity coupling algorithms. Fluid motion within the cavity is driven through shear forces provided by the translational motion of one or more of the bounding cavity surfaces. The *L*-shaped cavity introduced by Oosterlee *et al*. [13] is chosen for this work. The geometry for this cavity is detailed in Figure 2.

Arbitrary polygonal mesh topologies were used at three different cell densities. The coarsest mesh is shown in Figure 3. Numerical results are compared with the data provided by Oosterlee *et al*. [13] in Figures 4 and 5. Figure 4 compares the horizontal velocity along the vertical line D_v. The vertical velocity on the horizontal line D_h is compared in Figure 5. The finest mesh density, 6848 cells, matches the data provided by Oosterlee *et al*. [13].

9.1.1. 90° *cylindrical elbow.* Laminar flow through a smooth 90° cylindrical elbow was chosen for a three-dimensional evaluation of the proposed algorithm. The velocity and pressure distributions through this geometry are strongly three dimensional. The stream-wise velocity along the pipe is influenced by the secondary currents in the pipe cross-section due to centrifugal forces generated by the bend curvature. Enayet [14] has studied this flow experimentally and has provided stream-wise

DOI: 10.1002/fld

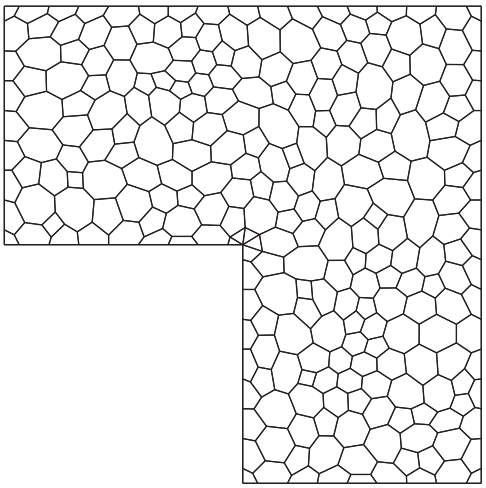

Figure 3. Coarse polygonal mesh topology.

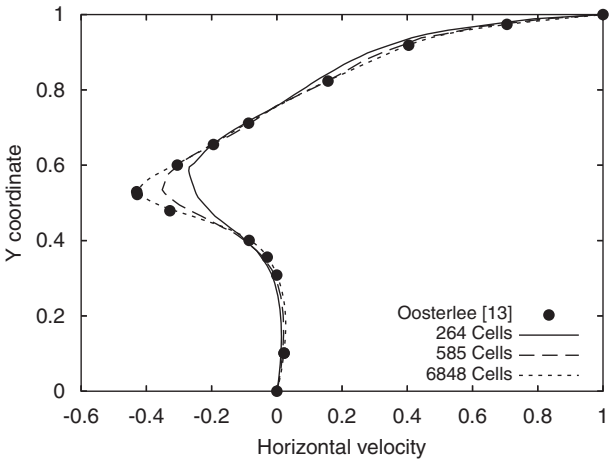

Figure 4. Horizontal velocity on line D_V.

velocity data along the centerline of the pipe. He and Salcudean [15] have presented numerical comparisons to this data using a curvilinear mesh topology.

The geometry of the experimental set up is outlined in Figure 6, where D was chosen to be 1 in this work. A uniform inlet velocity of 1 was used along with a fluid density of 1 and a viscosity of 0.002 to replicate the laminar Reynolds number of 500 documented by [14]. Four different mesh densities were investigated using fully arbitrary polyhedral mesh topologies. The mesh densities varied between a coarse mesh of 3180 control volumes to a fine mesh of 586 858 control volumes. The coarsest surface mesh is shown in Figure 7 and a close up of the finest density mesh is shown in Figure 8.

DOI: 10.1002/fld

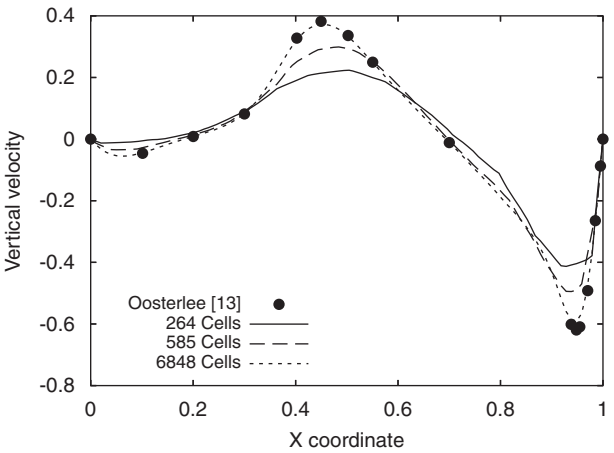

Figure 5. Vertical velocity on line D_{h}.

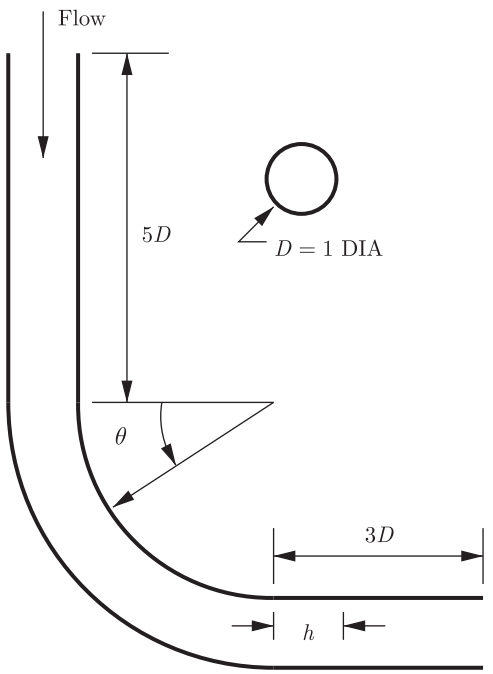

Figure 6. 90° cylindrical elbow geometry.

9.1.2. Comparison with experimental data. Figures 7–12 compare the current computational results to the experimental data of [14]. Each figure details the stream-wise velocity at the centerline of the pipe through the cross-section of the pipe. The velocity profiles shown in Figures 9–11 show how the velocity pattern transitions from a nearly parabolic fully developed profile at $\Phi = 30$ to a

DOI: 10.1002/fld

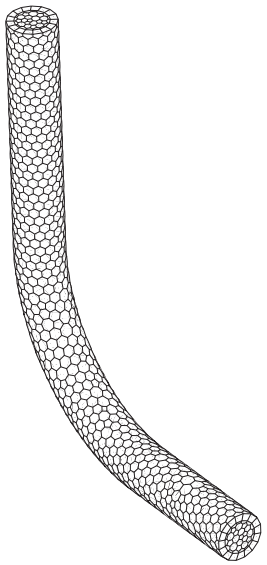

Figure 7. Coarse mesh topology.

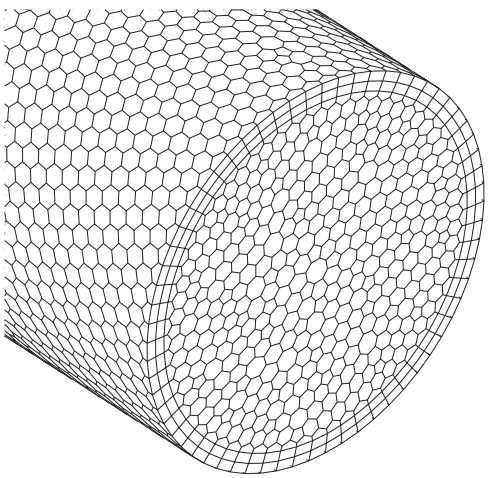

Figure 8. Fine mesh topology.

skewed profile at $\Phi = 75$ due to the bend geometry. The velocity profile at $h = D$, see Figure 12, indicates how the velocity distribution has begun its transition back to a fully developed profile. The finest mesh density predicts the velocity transitions throughout this geometry well, demonstrating the validity of the proposed algorithm.

9.1.3. Comparison with commercial software. To evaluate the convergence rate and relative numerical accuracy of the existing algorithm comparisons were made with the commercially available

DOI: 10.1002/fld

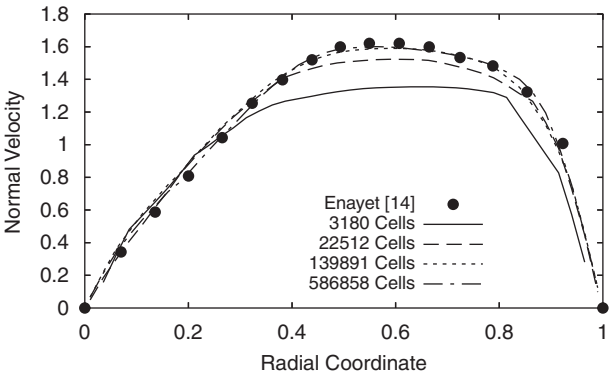

Figure 9. Correlation at $\theta = 30$.

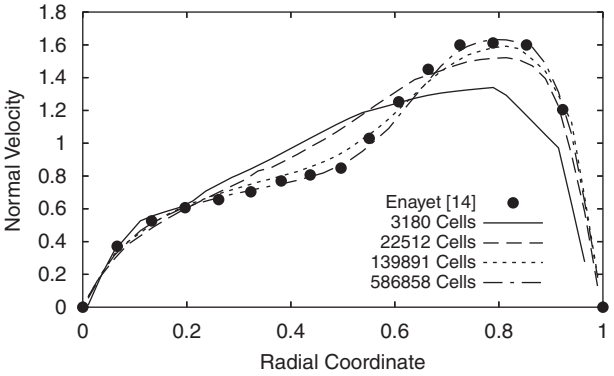

Figure 10. Correlation at $\theta = 60$.

software Fluent (version 6.3.26). The same exact mesh topology, 139 891 cells, was used for the comparison. The steady state SIMPLE algorithm was chosen in the Fluent software along with the second-order accurate discretization for the convective velocity and pressure gradients. The relaxations selected for this work were also chosen in Fluent (which happens to be the defaults recommended by Fluent). Figures 13 and 14 show the convergences rates for the absolute residuals R_Φ and R_{mass}. Comparisons of these two figures indicate that the proposed algorithm is competitive with the observed convergence rates of the Fluent software package.

Figure 15 shows the simulation results for Fluent and the proposed algorithm at the $\theta = 75$ location. These results show that the proposed algorithm predicts the solution to the same level of accuracy as Fluent. Only one line plot is shown in this paper but it should be noted that all sections showed the same level of agreement between Fluent and the current algorithm.

9.2. Particle-driven cavity

The algorithm proposed in this paper has been designed to handle traditional flow fields as well as multi-physics applications such as gas–particle flows. As mentioned before this type of system

DOI: 10.1002/fld

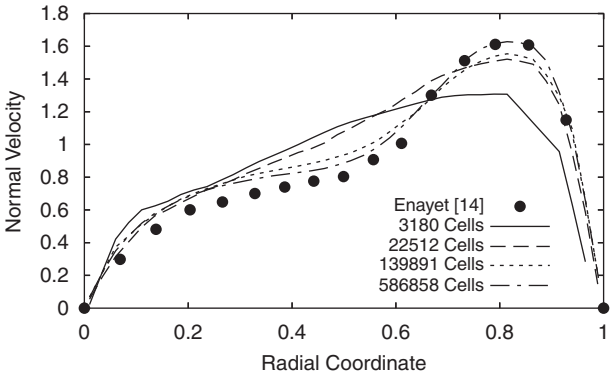

Figure 11. Correlation at $\theta = 75$.

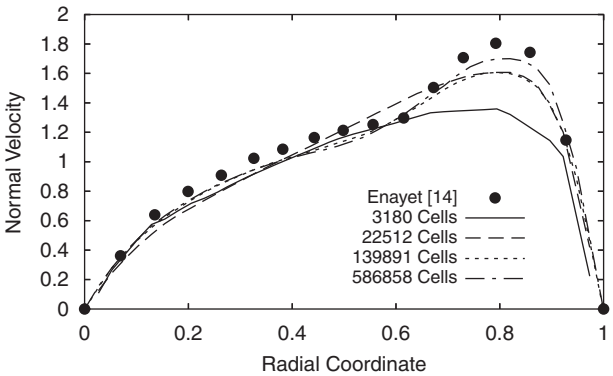

Figure 12. Correlation at location $h = D$.

adds additional non-linearities through coupling source terms which link the primary fluid to the secondary physics. To demonstrate the strength of this algorithm an idealistic two-dimensional gas/particle system is proposed. This system provides a test case similar in concept to the lid-driven cavities, where a cavity of fluid is driven in a circular motion by particle movement rather than wall shear forces.

Figure 16 shows a schematic of the proposed particle-driven cavity. A continuous uniform distribution of particles is introduced as indicated at the top of the cavity. These particles travel at a uniform velocity through the cavity staying within the shaded region indicated. When the particles reach the opposite side of the cavity they are removed from the system.

9.2.1. Phase coupling momentum source terms. The driving force for fluid motion in this cavity is due to the drag force of the particulate passing through the fluid. To couple the fluid phase with the particulate phase additional force terms, F_i, are included in the fluid momentum equation, see Equation (10). These force terms are equal and opposite in direction to the drag force of the fluid acting on the particulate.

DOI: 10.1002/fld

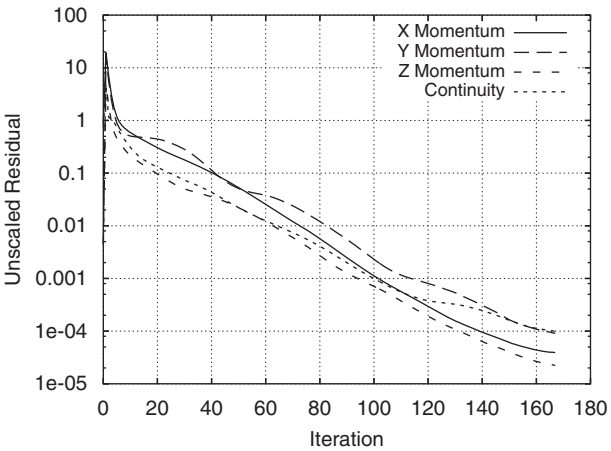

Figure 13. Un-scaled residuals for current algorithm.

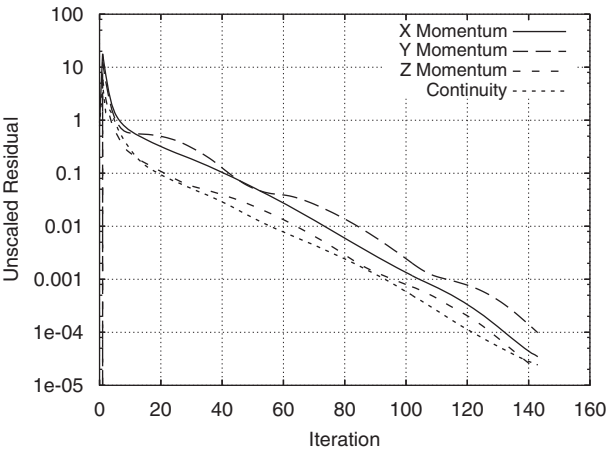

Figure 14. Un-scaled residuals observed from Fluent.

To include the particulate force terms in the momentum equation the drag force will be written using the standard form, see Equation (9). Equation (33) is used to represent the force relationship for each component of the Cartesian momentum equations.

$$F_i^{\text{particle}}(u_{i,p}) = F_i^{\text{explicit}} + F_i^{\text{implicit}} u_{i,p} \tag{33}$$

where F_i^{particle} is the drag force acting on the fluid in the Cartesian direction i. Note that this source term is a linearized function with respect to the centroidal velocity component, $u_{i,p}$. The implicit and explicit terms for this equation can be derived from the drag relationship between the particulate and the fluid. The linearized portion of this relationship is typically based on the relative slip velocity between the fluid and particle velocities.

DOI: 10.1002/fld

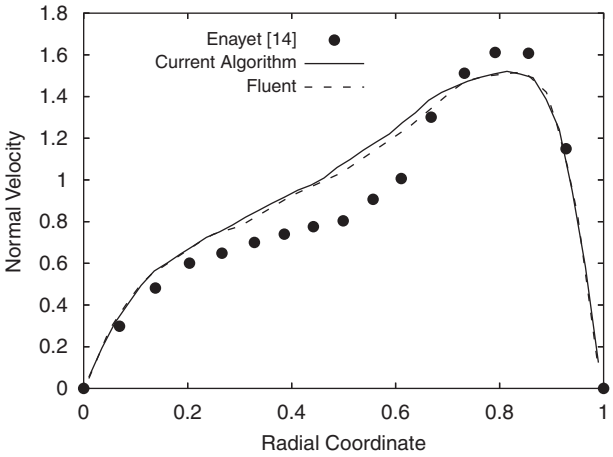

Figure 15. Correlation at $\theta = 75$.

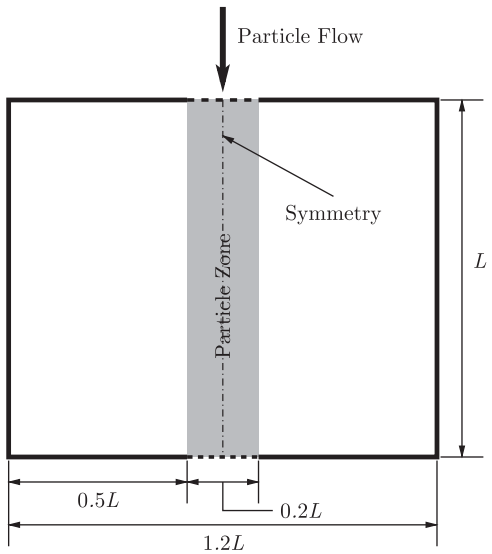

Figure 16. Particle-driven cavity.

For this test case we will consider a one-way-type coupling, where the particulate motion will be considered constant throughout the particle zone and will only influence the motion of the fluid in the vertical direction. A simple form of the momentum source term, F_y^{particle}, will be assumed by noting that the fluid velocity will tend toward the particulate velocity. The strength of this tendency will be dictated by the relationship between the implicit and explicit terms of Equation (33).

DOI: 10.1002/fld

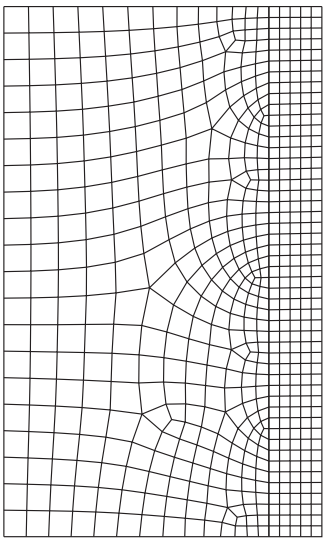

Figure 17. Mesh topology.

Table I. Source term constants.

Case number	F^{y}_{explicit}	F^{y}_{implicit}
1	50	−50
2	100	−100
3	150	−150
4	200	−200

9.2.2. Test case setup. The numerical stability of the proposed algorithm is compared with the treatment suggested by Mathur and Murthy [4], see Equation (34). The $\overline{\forall n_i n^i / A_p^{u_i}}$ term present in the proposed algorithm, see Equations (26) and (29), is replaced with Equation (34), where N is the dimension of the system (2 or 3):

$$\frac{\overline{\forall n_i n^i}}{\overline{A_p^{u_i}}} = \frac{\overline{N\forall}}{\overline{\sum_{i=1,N} A_p^{u_i}}} \tag{34}$$

Half of the cavity shown in Figure 16 was modeled taking advantage of the symmetry of the system. A two-dimensional 597 control volume mesh, see Figure 17, was used for the analysis. The fluid properties of standard air were used, $\rho = 1.225\,\text{kg/m}^3$ and $\mu = 1.7894\,\text{kg/(m s)}$.

A particulate velocity of 1 m/s was assumed and the driving force of F_y^{particle} was varied as shown in Table I. Note that each case has an implicit/explicit pair which drives the momentum source to zero when the primary control volume velocity, $u_{y,p}$, approaches 1 m/s. Conversely, when the primary velocity is not 1 m/s then the momentum source has a non-zero value. The strength of this source varies between each of the cases proposed.

DOI: 10.1002/fld

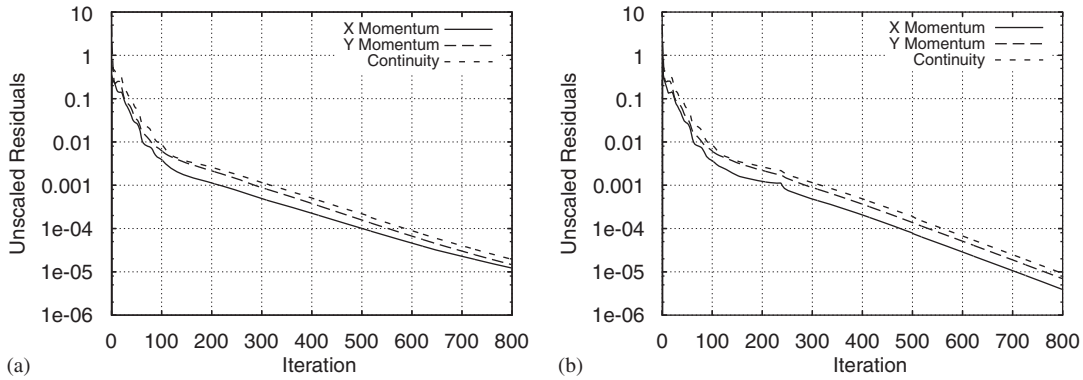

Figure 18. Residuals (Case 1): (a) $A_p^{u_i}$ method: averaging and (b) $A_p^{u_i}$ method: proposed.

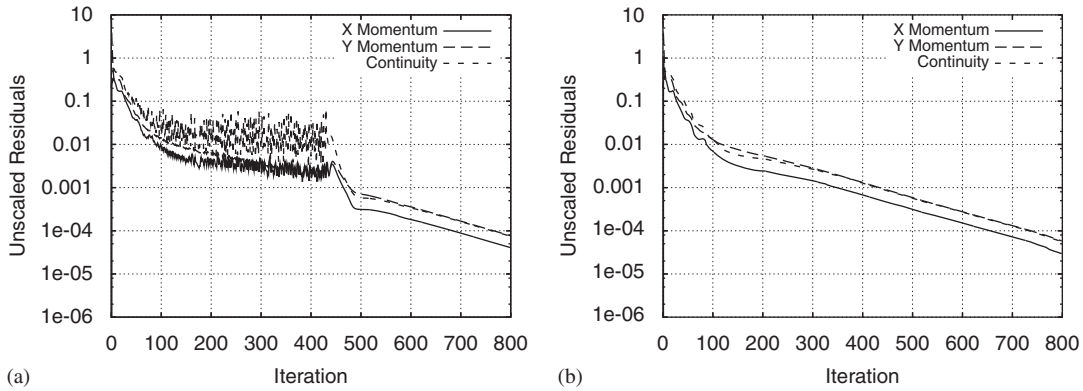

Figure 19. Residuals (Case 2): (a) $A_p^{u_i}$ method: averaging and (b) $A_p^{u_i}$ method: proposed.

Each case proposed in Table I introduces a stronger source term and therefore increases the non-isotropic nature of the $\overline{\forall n_i n^i / A_p^{u_i}}$ terms. Figures 18–21 trace the convergence rates for each of these cases.

The residuals for Case 1, Figure 21, show well-behaved convergence rates for both methods with the proposed method converging at a slightly faster rate. Instabilities begin to appear in Case 2 for the averaging method. The instabilities become more pronounced in Cases 3 and 4 for the averaging technique whereas the proposed algorithm remains stable and well behaved.

This series of cases highlight the importance of treating the $\overline{\forall n_i n^i / A_p^{u_i}}$ correctly. The proposed method retains the directional influence of the momentum source terms. This insures that the resulting pressure correction distribution from Equation (26) senses the non-isotropic nature of the momentum source, providing the proper projection of a new pressure distribution. The face velocity corrections, Equation (29), must also sense the non-isotropic nature and therefore it is important to treat the $\overline{\forall n_i n^i / A_p^{u_i}}$ term consistent with that used in Equation (26).

DOI: 10.1002/fld

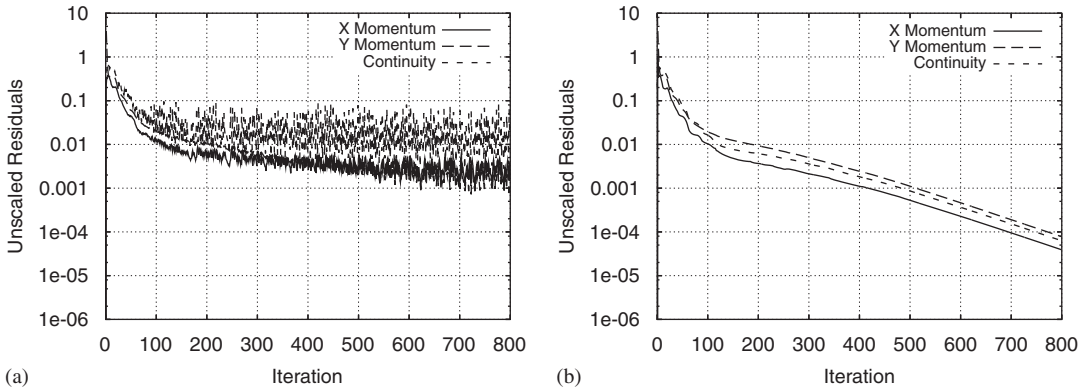

Figure 20. Residuals (Case 3): (a) $A_p^{u_i}$ method: averaging and (b) $A_p^{u_i}$ method: proposed.

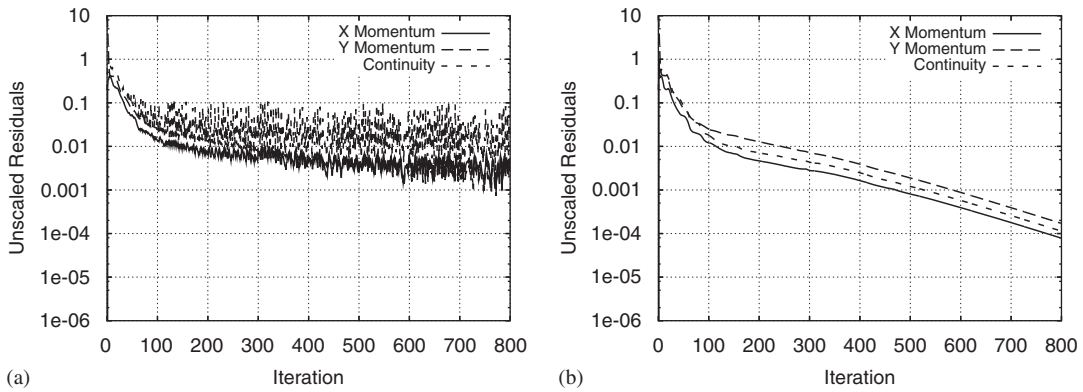

Figure 21. Residuals (Case 4): (a) $A_p^{u_i}$ method: averaging and (b) $A_p^{u_i}$ method: proposed.

10. CLOSING REMARKS

This work details a SIMPLE-based colocated pressure correction algorithm. The development of the proposed algorithm treats the coupling of the momentum and continuity equations in a general yet consistent form. The source of the commonly referred fourth-order pressure damping is detailed as the m_c term in this work. Two classical bench marks are used with fully arbitrary polygonal/polyhedral mesh topologies demonstrating the applicability and competitiveness of the current algorithm with existing implementations (Fluent). A new benchmark case was used to clearly show the importance of correctly treating the SIMPLE-based coupling when arbitrary grid structures and multiphase flows are present.

DOI: 10.1002/fld

NOMENCLATURE

Scalars

A	surface area
$A_p^{u_i}$	momentum equation i diagonal matrix coefficient
$A_f^{u_i}$	momentum equation i off diagonal matrix coefficient
F	force
p	static pressure
p'	pressure correction
Q^{u_i}	momentum equation i explicit term
S	control volume surface
S_Φ	scalar Φ source term
t	time
$\forall$	volume
ρ	density of the fluid
Φ	scalar variable
Γ	diffusion coefficient
α	momentum relaxation

Vectors

$\mathbf{n}, n_i$	control volume face normal unit vector
$\mathbf{s}, s_i$	control volume face tangent unit vector perpendicular to **n** and **t**
$\mathbf{t}, t_i$	control volume face tangent unit vector perpendicular to **n** and **s**
$\mathbf{u}, u_i$	fluid velocity

Subscripts

f	control volume surface
i	cartesian direction
p	primary control volume variable

REFERENCES

1. Patankar SV. *Numerical Heat Transfer and Fluid Flow*. Hemisphere Publishing Corporation: New York, 1980.
2. Patankar SV, Spalding DB. A calculation procedure for heat mass and momentum transfer in three dimensional parabolic flows. *International Journal of Heat and Mass Transfer* 1972; **15**:1787–1806.
3. Chow WL, Rhie CM. A numerical study of the turbulent flow past an isolated airfoil with trailing edge separation. *Technical Report AIAA-82-0998*, Center for Turbulence Research, 1982.
4. Mathur S, Murthy JY. A pressure-based method for unstructured meshes. *Numerical Heat Transfer*, *Part B* 1997; **31**:195–215.
5. Ferziger JH, Perić M. *Computational Methods for Fluid Dynamics*. Springer: Germany, 1997; corrected Second Printing.
6. Date AW. Fluid dynamical view of pressure checkerboarding problem and smoothing pressure correction on meshes with colocated variables. *International Journal of Heat and Mass Transfer* 2003; **46**:4885–4898.
7. Snider DM. An incompressible three-dimensional multiphase particle-in-cell model for dense particulate flows. *International Journal of Computational Physics* 2001; **170**:523–549.

DOI: 10.1002/fld

8. Leonard B. A stable and accurate convective modelling procedure based on quadratic upstream interpolation. *Computer Methods in Applied Mechanics and Engineering* 1979; **19**:59–98.
9. Jasak H, Weller HG, Gosman AD. High resolution nvd differencing scheme for arbitrarily unstructured meshes. *International Journal for Numerical Methods in Fluids* 1999; **31**(2):431–449.
10. Darwish MS, Moukalled F. TVD schemes for unstructured grids. *International Journal of Heat and Mass Transfer* 2003; **46**:599–611.
11. AIAA. A multi-dimensional linear reconstruction scheme for arbitrary unstructured Grids. *Sixteen AIAA Computational Fluid Dynamics Conference*, Orlando, FL, 23–26 June 2003.
12. Jasak H. Error analysis and estimation for the finite volume method with applications to fluid flow. *Ph.D. Thesis*, Department of Mechanical Engineering, Imperial College of Science, Technology and Medicine, June 1996.
13. Oosterlee CW, Wesseling P, Segal A, Brakkee E. Benchmark solutions for the incompressible Navier–Stokes equations in general coordinates on staggered grids. *International Journal for Numerical Methods in Fluids* 1993; **17**:301–321.
14. Enayet MM, Gibson MM, Taylor AMKP, Yianneskis M. Laser-doppler measurements of laminar and turbulent flow in a pipe bend. *International Journal of Heat and Fluid Flow* 1982; **3**:213–219.
15. He P, Salcudean M. A numerical method for 3D viscous incompressible flows using non-orthogonal grids. *International Journal for Numerical Methods in Fluids* 1994; **18**:449–469.

DOI: 10.1002/fld